Acta Metallurgica Sinica (English Letters) (2024) 37:54–66
https://doi.org/10.1007/s40195-023-01573-0

Comparative Study of 3D-Printed Porous Titanium Alloy with Rod Designs of Three Different Geometric Structures for Orthopaedic Implantation

Jiaxin Li[1,2] · Haozhang Zhong[3] · Bojun Cao[2] · Zhaoyang Ran[2] · Jia Tan[2] · Liang Deng[2] · Yongqiang Hao[2] · Jinglong Yan[1]

Received: 7 April 2023 / Revised: 18 April 2023 / Accepted: 28 April 2023 / Published online: 8 July 2023

Abstract
Porous titanium alloy is currently widely used in clinical treatment of orthopaedic diseases for its lower elastic modulus and ability to integrate with bone tissue. At the micro-level, cells can respond to different geometries, and at the macro-level, the geometric design of implants will also affect the biological function of cells. In this study, three kinds of porous scaffolds with square, triangular and circle rod shapes were designed and 3D printed. This study observed the proliferation and differentiation of MC3T3-E1 cells during surface culture of the three types of scaffolds. It also evaluated the characteristics of the three scaffolds by means of compression tests and scanning electron microscopy to provide a reference for the design of porous titanium alloy implants for clinical applications. The trends of cell proliferation and gene expression between the three types of scaffolds were observed after treatment with two inhibitors. The results show that the square rod porous scaffolds have the best proliferative and osteogenic activities, and these findings may be due to differences in piezo-type mechanosensitive ion channel component 1 (Piezo1) and Yes-associated protein (YAP) expression caused by the macro-geometric topography.

Keywords Porous titanium scaffolds · Geometric morphology · Cell proliferation · Structural design

1 Introduction

Bone regeneration and reconstruction have always been important topics in the biomedical field. For a large bone defect that cannot heal by itself, it is necessary to use implants to fill the defect area and to encourage cells to migrate into the defect area, proliferate, differentiate and develop into new bone. Traditional implants are mostly autogenous or allogeneic bone transplants, but there are some inevitable problems, such as collateral injury, limited bone mass and transmitted diseases. Therefore, research on artificial bone repair materials has emerged in recent years. Ti6Al4V alloy has been widely used in orthopaedic implants due to its excellent mechanical strength, corrosion resistance and good biocompatibility, and it has become the most commonly used material for orthopaedic medical devices since it was invented.

The elastic modulus of human cortical bone is approximately 5–15 GPa, that of cancellous bone is approximately 0.2–5 GPa [1, 2], and that of the Ti6Al4V alloy can reach 110 GPa. Therefore, in the early days, when it was used for bone implants, it often faced the problem of stress shielding, which affected the regeneration and reconstruction of bone tissue. To solve such problems, the concept of elastic fixation has been introduced in the field of orthopaedic treatment so that the damaged part of the bone tissue can bear a certain mechanical load, stimulating bone tissue regeneration [3].

Jiaxin Li and Haozhang Zhong have contributed equally to this work.

Available online at http://link.springer.com/journal/40195

✉ Yongqiang Hao
676471883@qq.com

✉ Jinglong Yan
yjlhmu@163.com

[1] Department of Orthopedics, The Second Affiliated Hospital of Harbin Medical University, Harbin 150001, China

[2] Shanghai Engineering Research Center of Innovative Orthopaedic Instruments and Personalized Medicine, Shanghai Ninth People's Hospital, Shanghai Jiao Tong University School of Medicine, Shanghai 200011, China

[3] Institute of Materials Modification and Modeling, Shanghai Jiao Tong University, Shanghai 200240, China

Compared with the traditional methods of preparing porous metal materials, porous implants prepared by selective laser melting (SLM) and electron beam melting (EBM) technology can be freely adjusted in terms of porosity, pore size and pore morphology, and the arrangement of the porous structure is precise and controllable [4]. Since the advent of porous Ti6Al4V bone implants, researchers have long been committed to finding a porous implant design more conducive to bone tissue regeneration. Bone implants need to repeatedly withstand complex and varied biological stresses during rehabilitation exercises and daily activities. Therefore, in addition to improving performance by optimizing the manufacturing process [5], the design of porous bone implants that aims to improve biological effectiveness can be particularly critical. Although increasing porosity can promote the integration of implants into bone tissue, increasing porosity under the same structural design will result in significant mechanical property degradation [6].

Therefore, implant structural design has attracted the attention of researchers. The initial design concept of porous implants was to improve mechanical properties, so manufacturers choose diamond structure, tetrahedral structure and other lattices [7], and all these designs mainly optimizing some parameters. Studies of pore size have shown that porous Ti6Al4V metal implants with a pore size of 300–400 μm achieve the best bone tissue regeneration performance [8], and studies on pore morphology have shown that concave pores with greater curvature can lead to a greater cell proliferation rate and tissue deposition thickness [9]. Cells can sense geometric cues ranging from nanometres to millimetres through cytoskeleton and cell surface mechanical signalling-related proteins [10], and these cues subsequently produce various corresponding biological effects. There have been a large number of studies on geometric cues at the micro- and nanoscale [11–13].

However, on the macroscale, in addition to the pore shape, the single filament of the scaffold cell unit serves as the surface for the cells to adhere to and grow, and its morphology may also have a significant impact on the mechanical properties of an additively manufactured porous material. Whether cell growth and tissue deposition will produce corresponding biological effects remains to be further studied. Therefore, we chose square, triangular, and circular cross-sectional single-cell filaments with three different curvatures to prepare additively manufactured porous Ti6Al4V as the research object. MC3T3-E1 cells are the precursor cells of mouse osteoblasts, which can maintain a relatively stable cell phenotype after multiple passages, and have the potential of osteogenic differentiation. Therefore, MC3T3-E1 cells are often used in the field of orthopaedic biomaterials. We studied the process of surface cell growth and differentiation and then detected the relative expression levels of several genes related to mechanical signals and cell proliferation to clarify its potential mechanism. This study provides a reference for the design of additively fabricated porous Ti6Al4V bone implants. Although porous titanium alloy implants have been widely used in clinical practice, there is no unified specification and standard for the design of porous structures. Because of its excellent mechanical properties, lattice composed of diamond structures with cylindrical rods have become a commonly used design in clinical practice [14]. At present, the pore size and porosity of porous implants have been fully studied. Research on lattice structure design focuses more on mechanical properties (including anisotropy and gradient structure), permeability, etc. [15, 16], while there are relatively few researches on biology. It is rare to report that the rod structure directly attached to cells can affect both mechanical and biological properties. Therefore, based on the SLM implant processing technology for clinical application, we designed three different forms of rod structure scaffolds. After evaluating through the experimental methods as shown in Fig. 1, the effects of three different rod structure designs on cells were observed from the biological point of view, and the rod geometry design of porous scaffolds suitable for bone implants was selected.

2 Experimental

2.1 Preparation of Porous Scaffolds with Different Geometric Structures

Different geometric structure Ti6Al4V porous scaffolds were manufactured using an SLM system (FS121M, Farsoon Technologies, China) through 3D printing technology. The quality requirements of Ti6Al4V powder are less than 500ppm oxygen content and less than 300 ppm nitrogen content. Three kinds of rod-shaped cells, namely square, triangle and circle lattices, were created by stretching three different cross sections and mirroring them multiple times, the array was arranged subsequently. The 3D models of the porous scaffolds that have different geometric structures with a square, triangle and circle intersecting surface were generated through SolidWorks software (Fig. 2a–c). The models were transmitted to the 3D printer with computer-aided manufacturing (CAM) software in the form of an STL format file. The particle size of the powder ranged from 20 to 40 μm. The laser melted the metal powder, and then, the metal was coagulated. A new layer of powder was then spread to form the next layer and so on until the whole structure was formed. The entire manufacturing process was conducted in a vacuum environment. After 3D printing, the porous scaffolds were cut

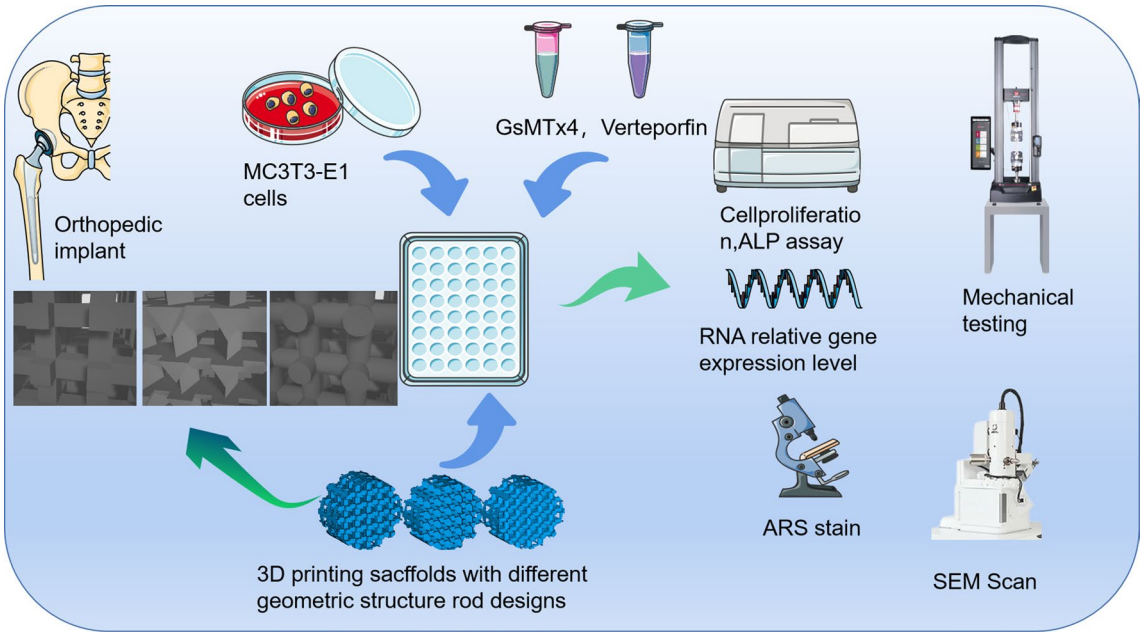

Fig. 1 Schematic diagram of main research methods

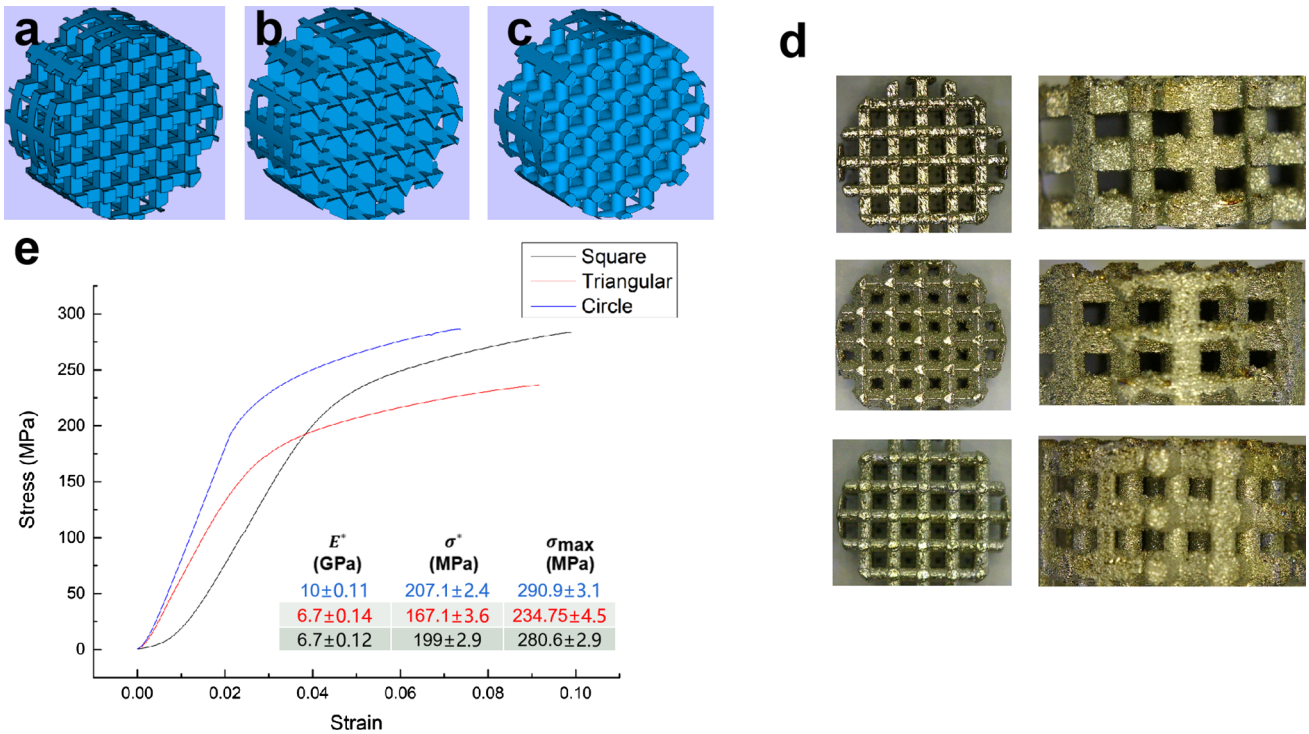

Fig. 2 Preparation and characterization of porous scaffolds with different rod geometric designs: **a–c** design drawing display, **d** general picture of porous scaffold, **e** stress–strain curves of 3 kinds of scaffolds

from the substrate by a wire cutter after an excess powder removal step.

The porous scaffolds (Ø9 mm × L5 mm) used for in vitro experiments (shown in Fig. 2d) underwent ultrasonic washing to remove any residual metal powder.

2.2 Mechanics Performance Testing

The scaffold compression test was carried out with the equipment of the Analysis and Test Centre of Shanghai Jiao Tong University (Instron 5966, USA.), and the sample size was a cube of 10 mm × 10 mm × 20 mm. The compression load was carried out at a rate of 2 mm/min until the porous scaffold became plastic. Four samples in each group were measured to obtain the average stress−strain curve. The elastic modulus was calculated using the value of 2% strain in the initial linear region.

2.3 Cell Culture

The MC3T3-E1 cell line was used in the following experiments. MC3T3-E1 cells were cultured in α-MEM (HyClone, Grand Island, NY) supplemented with 10% foetal bovine serum (FBS, Gibco, Tauranga, New Zealand) at 37 °C in a moist atmosphere with 5% CO_2. The α-MEM medium was changed every 2 days. Passaging was performed when the degree of cell fusion reached 80–90%.

2.4 Cell Viability and Morphology on Different Geometric Structures of Ti6Al4V Porous Scaffolds

The proliferation of MC3T3-E1 cells on the different geometric structure Ti6Al4V porous scaffolds was evaluated with a Cell Counting Kit-8 assay (Dojindo Molecular Technology, Japan) as previously described ($n = 5$). Sterile porous scaffolds were placed in a 48-well cell culture plate. Then, 0.5 ml of MC3T3-E1 cell suspension was added to each well at a density of 4×10^3 cells/ml, and the culture medium was renewed every 48 h. After 1, 3 and 5 days of culture at 37 °C in a moist atmosphere with 5% CO_2, Cell Counting Kit-8 solution was added to the culture medium at a ratio of 1:10. Following the manufacturer's instructions, the cells were incubated for 2 h, and the optical density at 450 mm was measured using a microplate reader (Thermal Fisher Instruments Inc., USA). The experiments were repeated three times, with five samples per group in each experiment.

2.5 Cell Adhesion Characterization

MC3T3-E1 cell suspensions were seeded on the different geometric structure Ti6Al4V porous scaffolds at a density of 4×10^3 cells/ml and cocultured with the method described above, and the α-MEM medium was changed every two days. Then, the medium was removed. The scaffolds were washed with phosphate buffer solution twice and then fixed in 4% paraformaldehyde solution for 30 min at 4 °C. Next, the samples were washed with phosphate buffer solution again. The cytoskeleton was stained with phalloidin (Cytoskeleton, PHDG1-A, USA) for 30 min at room temperature, the working solution was removed, and the samples were washed 3 times. The nuclei were stained with 4′,6-diamidino2-phenylindole (DAPI) solution for 10 min at room temperature, and then, the samples were washed following the same method. The samples were then observed and scanned by laser scanning confocal microscope (Leica TCS SP8 system, Wetzlar, Germany).

MC3T3-E1 cells were collected and seeded on 3D-printed porous scaffolds with different geometric structures. The cells were cocultured with the scaffolds for 7 days, and the medium was changed every 2 days. After 7 days of coculture, the cells adhered on the scaffolds were fixed with glutaraldehyde stationary liquid (Solarbio, China) and then dehydrated with different concentrations of ethanol (50%, 60%, 70%, 80%, 90% and 100%). After sufficient drying, the surface of the support was sprayed with conductive adhesive to increase the electrical conductivity. A scanning electron microscope (SEM, TESCAN LYRA3 system Czech Republic) was used to observe the cells attached to the surface of the scaffolds. The voltage was set to 20 kV, and the scan was carried out at 30×, 150× and 1000× magnifications.

2.6 In Vitro Osteogenesis Assay

The osteogenic differentiation of MC3T3-E1 cells on porous Ti6Al4V scaffolds with different geometric structures was evaluated by alkaline phosphatase (ALP) activity tests and Alizarin red staining. The MC3T3-E1 cells were added to different geometric structures of Ti6Al4V porous scaffolds cocultured for 3 days. The α-MEM culture medium was removed, and osteogenic induction medium (OriCell Cyagen, USA) was added to the culture plate well, and the cells were cultured for 7, 14 and 21 days. The medium was changed every 2 days. After 7 and 14 days of coculture, the ALP activity in the culture medium was measured with an ALP activity detection kit (Beyotime Biotechnology, China). After a 21-day coculture with MC3T3-E1 cells in osteogenic induction medium, the samples were stained with Alizarin red stain solution (OriCell Cyagen, USA), and then imaged with a stereomicroscope (LeiCa M205 FA, Wetzlar, Germany); the magnification was set at 9×. The mineralized nodules were subsequently dissolved by cetyl pyridinium chloride (Solarbio, China), and the optical density (OD) value at 562 nm was measured with a microplate reader. All

experiments were repeated three times, with five samples per group in each experiment.

2.7 q-RT PCR Assay

The MC3T3-E1 and MG-63 cells were cocultured with different geometric structures of Ti6Al4V porous scaffolds for 14 days. The culture medium was removed, and the total RNA of MC3T3-E1 cells was extracted with TRIzol reagent. Total RNA was reverse transcribed to cDNA with a TaKaRa perfect RT MIX Kit. The expression of several molecular markers, including notch homolog 1 (Notch1), yes-associated protein (YAP), jagged 1 (Jag1), nuclear factor-k-gene binding (NF-KB), inhibitory subunit of nuclear factor-kappa B (I-KB), and piezo-type mechanosensitive ion channel component 1 (Piezo1), was detected by quantitative reverse transcription-polymerase chain reaction (RT−PCR) analysis. RT–PCR was performed using SYBR Premix Ex TaqII (Bimake) and 384 PCR plates (Axygen PCR-384-C, USA) with a Quant Studio™ 6 Flex System (Thermal Fisher Instruments Inc., USA). The housekeeping gene glyceraldehyde-3-phosphate dehydrogenase (GAPDH) was used as a control. The primer sequences were obtained with Oligo7 software. The primers were synthesized by Shanghai Sangong Biotechnology Co., Ltd. The primer sequences are shown in Table 1.

2.8 Inhibitor Treatment and Reassay

Two inhibitors were used in this research. The inhibitor of the Piezo1 signalling pathway Grammostola spatulata mechanotoxin 4 (GsMTx4) was added to the α-MEM cell culture medium at a concentration of 3 μM/L. MC3T3-E1 cells were seeded on porous scaffolds with different geometric structures of Ti6Al4V, the culture medium was replaced with α-MEM cell culture medium containing GsMTx4 the next day, and the cell proliferation test was performed as described above. The inhibitor of the YAP signalling pathway was added to the α-MEM cell culture medium at a concentration of 2 μM/L, and MC3T3-E1 cells were seeded on the scaffolds and tested as described for the other inhibitor.

3 Results

3.1 Mechanical Performance

The stress−strain curves of scaffolds with three different geometric shapes are shown in Fig. 2e. The results show that the compressive strength of the triangular rod intersecting scaffold is significantly lower than that of the other two groups, and the scaffolds with circular and square rod intersecting designs both have higher compressive strength. However, in terms of the elastic modulus, the scaffolds designed with intersecting triangular rods and square rods were obviously lower than that designed with circular rods. A previous study found that the size change of the rod in the EBM-printed porous titanium alloy scaffolds has a significant impact on the mechanical properties [17]. In this study, the difference in compressive strength between the square rod and the circle rod scaffolds is not significant, while the difference between the triangular rod and the other two designs is more obvious.

3.2 SEM and Laser Confocal Microscope Observation

Cell adhesion was detected on the surface of scaffolds with three different geometric designs, as shown in Fig. 3. The attachment of cells on a single rod of the scaffolds is shown in Fig. 4b–d. When seeded with MC3T3-E1 cells, the cells on the surface of square rod and triangle rod scaffolds were denser than those on the surface of circle rod intersecting scaffolds. All cells attached to the 3D-printed scaffolds were fully stretched. The cells distributed on the surface of the square rod intersecting scaffolds were denser than those on the other two designs. The surface of the square rod intersecting scaffold is the flattest, while the surface of the round rod intersecting scaffold has the most semimolten particles. The square rod scaffolds prepared by Peng et al. has smooth surface and fewer semimolten particles [18]. But in this study, the surface morphology and proliferation of the cell attached on the scaffolds were studied under the same process parameters and different rod designs.

Table 1 Primers used for quantitative RT-PCR analysis

Gene	Forward primer sequence (5′–3′)	Reverse primer sequence (3′–5′)
GAPDH	AGGTCGGTGTGAACGGATTTG	TGTAGACCATGTAGTTGAGGTCA
Notch1	GATGGCCTCAATGGGTACAAG	TCGTTGTTGTTGATGTCACAGT
YAP	GGCTCTAAAGAACCCGAACC	GCAGCTGAAGAAACCACCTC
Piezo 1	CACTGGCCCAGAGCTTCTAC	ATGTCTGTGGCTGCAGAGTG
Jag 1	TGCCTCTGTGAGACCAACTG	AGGGGTCAGAGAGACAAGCA
NF-KB	CTGACCTGAGCCTTCTGGAC	GCAGGCTATTGCTCATCACA

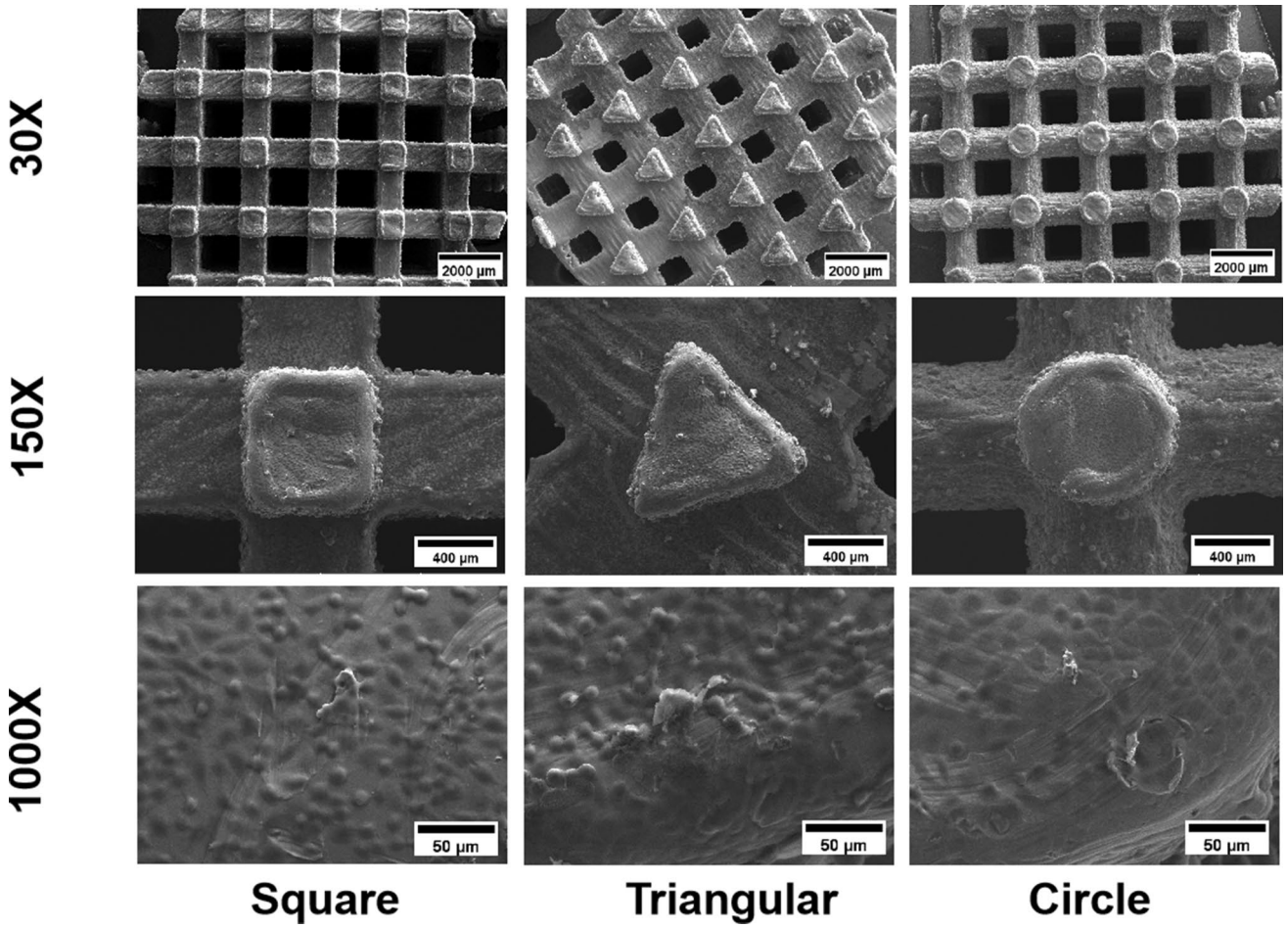

Fig. 3 Distribution of MC3T3-E1 cells on three scaffolds with different rod geometric structures (magnification 30×, 150× and 1000×)

3.3 Cell Proliferation on Porous Scaffolds with Different Geometric Structures

Figure 4a presents the cell proliferation results of MC3T3-E1 cells cocultured with porous scaffolds with different geometric structures, which showed an increasing trend in all three types of porous scaffolds as the incubation time increased. However, a discrepancy in the MC3T3-E1 cell proliferation rate was observed between the square, triangle and circle rod intersecting scaffolds. Square rod intersecting scaffolds had a relatively high cell proliferation rate. The cell proliferation rate was not significantly different between the other two types of intersecting scaffolds.

The same procedure was carried out using pore size-controlled porous scaffolds with different geometric structures and surface area-controlled porous scaffolds with different geometric structures. As shown in Figs. 4a and 5, all 3 series of porous scaffolds with different geometric structures produced the same result: The square intersecting scaffolds exhibited a relatively high cell proliferation rate. In a study of Thibeaux et al., the effect of different geometric materials on surface cell growth under simulated tissue perfusion conditions was evaluated [19], but there was a large gap between the method and the clinical application of porous implants, and the variables were not well controlled.

3.4 In Vitro Osteogenesis Assay

3.4.1 ALP Activity Assay

Figure 6a and b presents the ALP activity assay results. The ALP activity of MC3T3-E1 cells after 7 days and 14 days

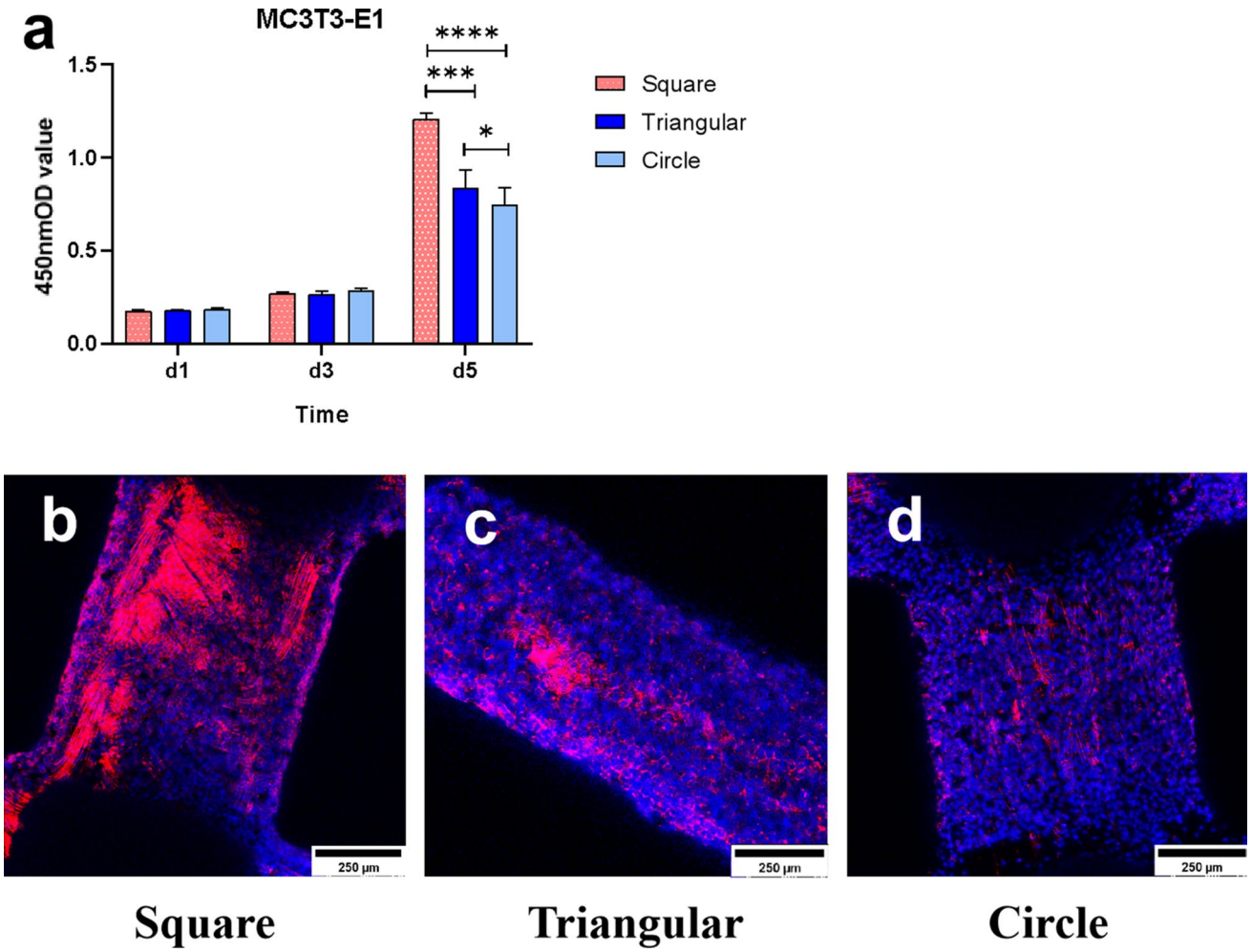

Fig. 4 Cell proliferation and adhesion on the surface of scaffolds designed with three different rod geometric structures: **a** cell proliferation of scaffolds designed with three different rod geometric structures, **b–d** confocal laser scanning images of MC3T3-E1 cells on the scaffold surface with three different geometric rod designs

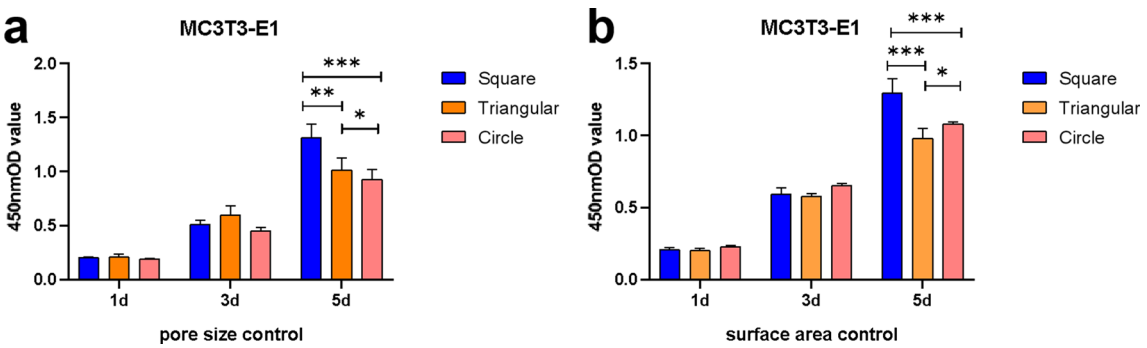

Fig. 5 Cell proliferation of scaffolds designed with the pore size control and surface area control of three different rod geometric structures: **a** cell proliferation of pore size control scaffolds designed with three different rod geometric design, **b** cell proliferation of surface area control scaffolds designed with three different rod geometric design

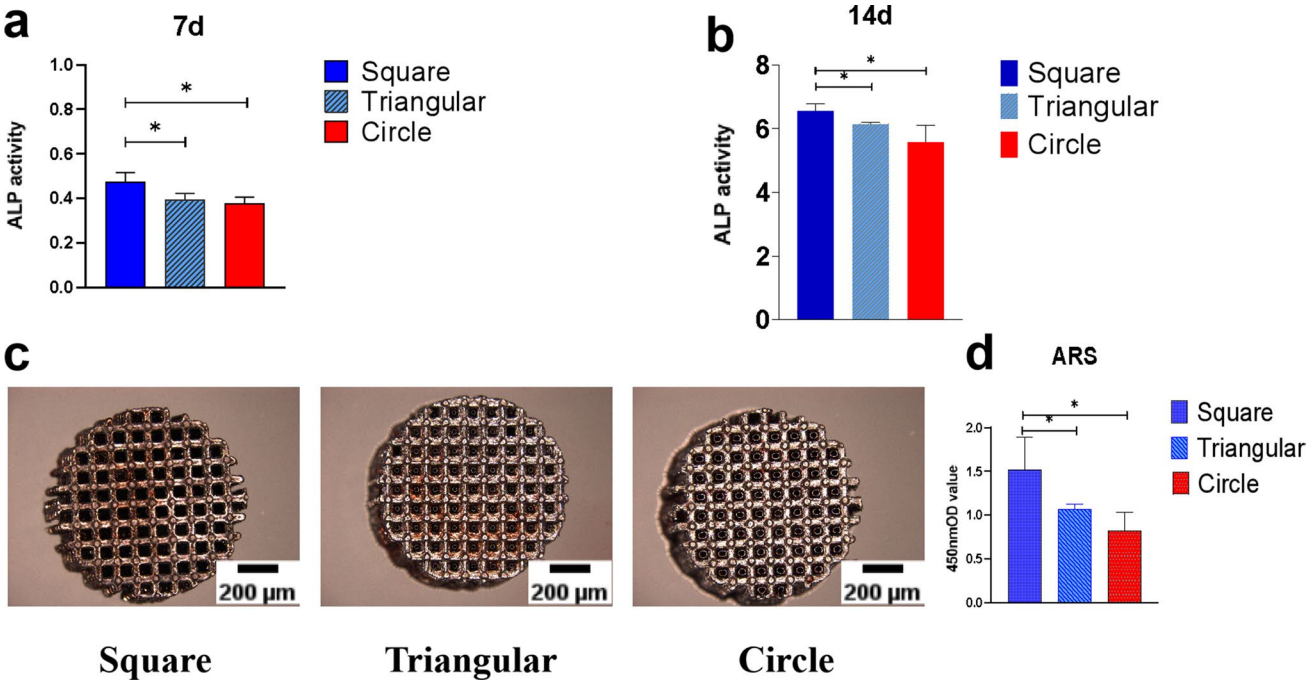

Fig. 6 Osteogenic activity of MC3T3-E1 cells on three scaffolds with different rod geometric structures: **a** alkaline phosphatase activity was different among different groups after 7 days of culture, **b** alkaline phosphatase activity was different among different groups after 14 days of culture, **c** alizarin red staining of MC3T3-E1 cells cultured on scaffolds with three different rod geometric designs, **d** semiquantitative detection of alizarin red

of coculture with the square rod intersecting scaffolds was significantly higher than that of the other two groups, and the cells cocultured with circle rod intersecting scaffolds exhibited the lowest ALP activity.

3.4.2 ARS Staining and Semiquantitative Assay

The Alizarin red staining results of porous scaffolds with different geometric structures are shown in Fig. 6c. All three groups of porous scaffolds exhibited the formation of mineralized nodules, and the semiquantitative assay showed that the square rod intersecting scaffolds exhibited the highest level of mineralization. The circle rod intersecting scaffolds had the lowest amount of mineralization, as shown in Fig. 6d. All of the above experimental results revealed that the MC3T3-E1 cells cocultured with the square rod intersecting scaffolds had higher levels of osteogenesis than the triangle rod intersecting scaffolds and the circle rod intersecting scaffolds. A previous study on the effect of topological optimization on osteogenic differentiation of bone marrow mesenchymal stem cells only studied the gene expression of early osteogenic differentiation from the gene level [20], but this study focused on the protein level and cell mineralization level, the results were more convincing.

3.5 Relative Gene Expression

After 14 days of coculture with porous scaffolds with different geometric structures, the total RNA of MC3T3-E1 cells was extracted. The relative expression levels of the Piezo1, Notch1, YAP, NF-KB, and Jag1 genes were detected. Figure 7 shows that for MC3T3-E1 cells cocultured with square rod intersecting scaffolds, the Piezo1, Notch1, YAP, NF-KB and Jag1 genes had a lower expression level than the other two groups.

3.6 Cell Proliferation on Porous Scaffolds with Different Geometric Structures after Treatment with the Inhibitors

After treatment with the Piezo1 signalling pathway inhibitor GsMTx4, a different cell proliferation pattern was observed. For the pore size control group, MC3T3-E1 cells cocultured with square intersecting scaffolds had the lowest cell proliferation rate, as shown in Fig. 8a, exactly the opposite of what it was without GsMTx4 treatment. For the cells cocultured with the surface area control group, the result is presented in Fig. 8b. Although the MC3T3-E1 cell proliferation rate was still the highest in the square intersecting scaffold group, the difference between the groups was smaller than that in the noninhibitor treatment group.

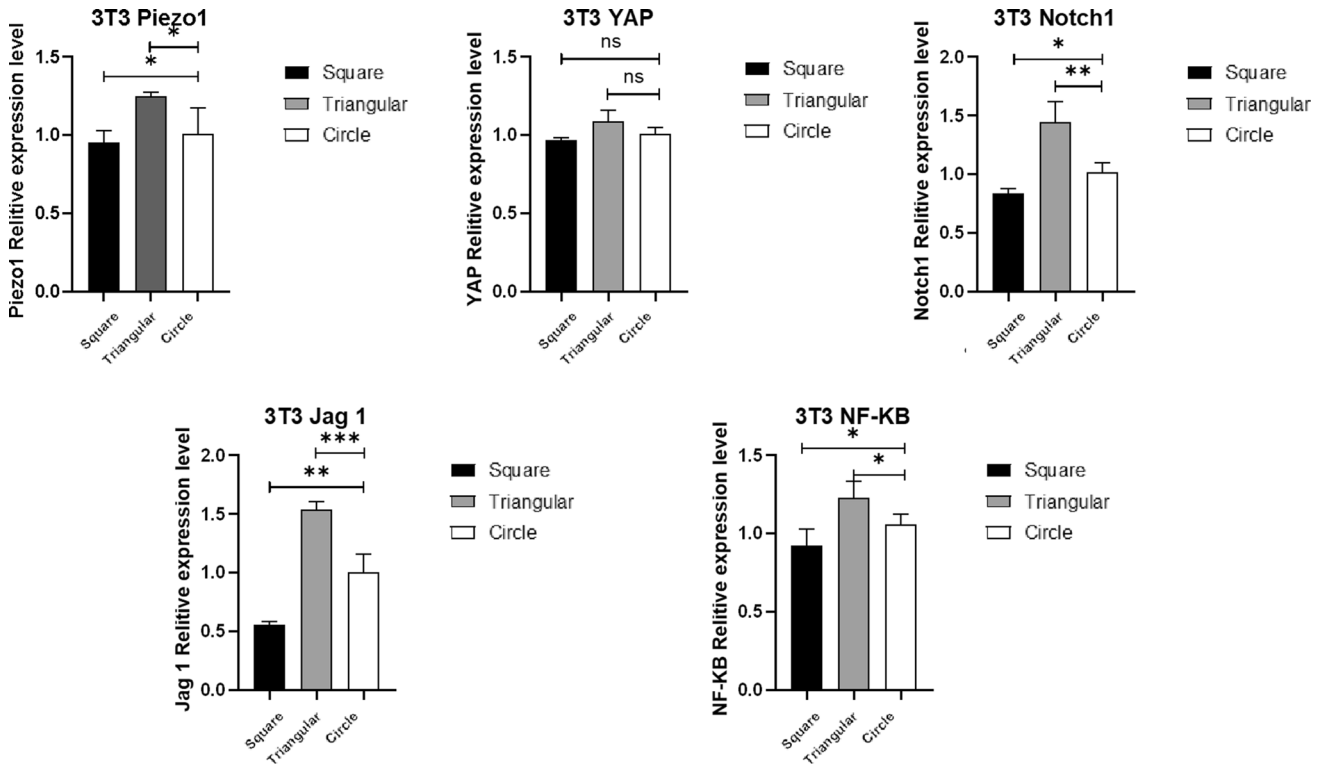

Fig. 7 Relative gene expression levels of MC3T3-E1 cells cultured on scaffolds designed with rods of three different geometric designs: relative gene expression levels of Piezo1, YAP, Notch1, Jag1 and NF-KB between three different scaffolds

When the cells were treated with verteporfin, an inhibitor of the YAP signalling pathway, a similar opposite trend in cell proliferation was observed. For the pore size control group, Fig. 8c shows that the MC3T3-E1 cell proliferation rate of square group changed from the highest to the lowest. While the cell proliferation rate of triangular group changed from lowest to the highest and the difference in MC3T3-E1 cell proliferation between the groups was smaller than that in the noninhibitor treatment group. In regard to the surface area control group, only small differences among the 3 groups were found, as shown in Fig. 8d.

3.7 Relative Gene Expression after Inhibitor Treatment

After treatment with inhibitors, the relative gene expression trend was changed. As shown in the RT−PCR results, in MC3T3-E1 cells, the square intersecting group had the lowest Piezo1, YAP, Jag1, Notch1 and NF-KB gene expression levels. However, when treated with GsMTx4, the expression levels of these five genes in the square rod intersecting group were converted to the highest level, as shown in Fig. 9. This pattern was consistent with the change in cell proliferation after the use of the inhibitor. Figure 10 presents the results of treatment with verteporfin. In MC3T3-E1 cells, differences in the expression of the YAP, Notch1, and Jag1 genes across the three different types of scaffolds became narrow, and the relative expression trends of the Piezo1 and NF-KB genes were reversed among the three groups.

4 Discussion

Although a variety of biomaterials are currently available for the manufacture of in vivo implants, titanium alloy is still the first choice for the manufacture of implanted medical devices due to its excellent biocompatibility and mechanical properties. But stress shielding is an unavoidable problem in bone implants field, researchers found that a moderate mechanical stimulation can promote bone regeneration [21]. A porous structure design can reduce the elastic modulus of the implant, and the appropriate design can effectively integrate with the bone tissue around the implant to avoid implant loosening, so it has been rapidly popularized and applied in clinical practice. There have been several studies on some common parameters affecting the performance of porous implants, including pore diameter, pore type and rod diameter [22–24]. However, the use of rods as the structure to which the cells are initially directly attached has not been widely reported. Surfaces with different curvatures have the ability to regulate the growth dynamics of cell tissue to a certain extent, and the macroscopic mechanical and physical

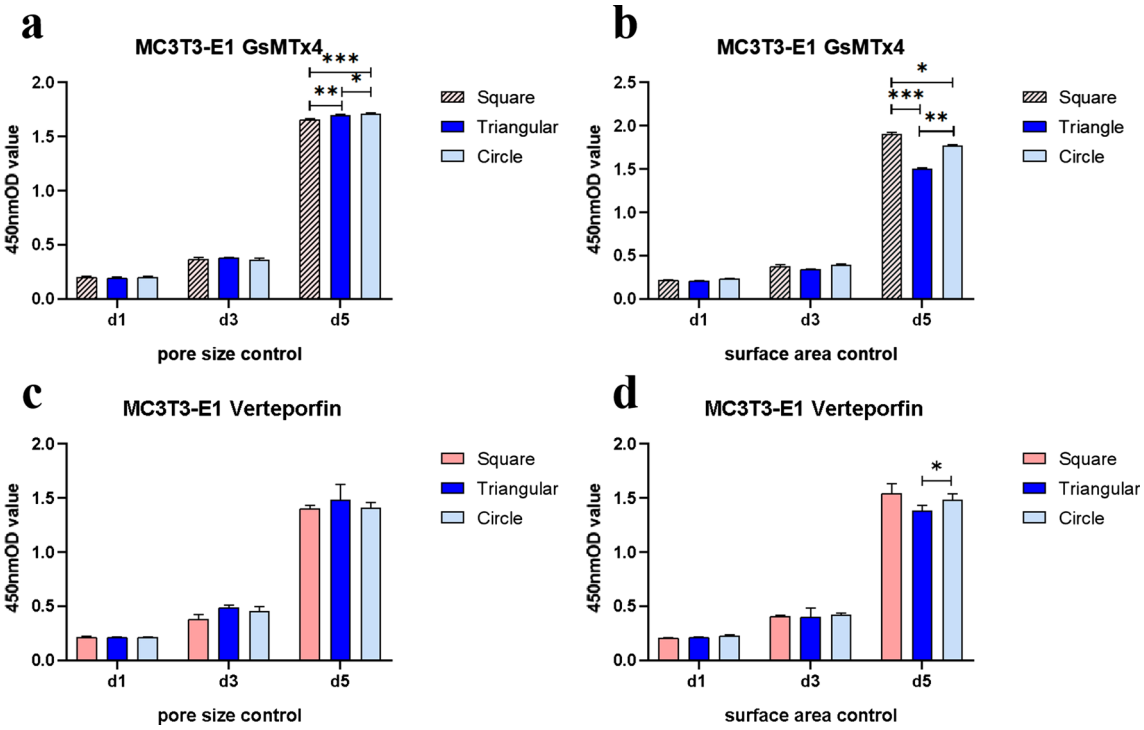

Fig. 8 Cell proliferation of scaffolds designed with the pore size control and surface area control of three different rod geometric structures after inhibitor: **a** cell proliferation of pore size control scaffolds designed with three different rod geometric designs after GsMTx4 treated, **b** cell proliferation of surface area control scaffolds designed with three different rod geometric designs after GsMTx4 treated, **c** cell proliferation of pore size control scaffolds designed with three different rod geometric designs after verteporfin treated, **d** cell proliferation of surface area control scaffolds designed with three different rod geometric designs after verteporfin treated

environment can also change the biological behaviour of cells [25, 26]. So we carried out the study based on the ideas expressed in Fig. 1.

In this work, we used MC3T3-E1 cells and obtained the best cell proliferation in square rod structures (Fig. 4a), which may be related to the fact that the cells tended to form boundaries with minimal surface tension [9]. A study on scaffold pore geometry found that scaffolds with a triangular structure had the best cell adhesion capacity [27]. Among the three scaffold structures involved in this study, the square rod structures have four flat faces, so any two faces at the intersection of the rods can form a triangular cross-sectional area with a certain thickness, which has been shown in previous studies to be a structure that supports relatively rapid cell growth. In recent years, triply periodic minimal surfaces (TPMS) structure has become a research hotspot in metal structure design [28]. We also prepared implants with this structure in the initial preliminary experiment. However, there are still many limitations in the preparation of this complex curved structure with the technology used in the current clinical application of implants, the surface of the implant is still rough, and the residual metal powder inside the structure can be more difficult to remove.

The growth of cells is affected by many factors, such as matrix roughness, stiffness, and fluid shear stress [29]. Two adjacent parallel rods of a square rod scaffold may have obvious fluid shear stress shielding in the same horizontal or vertical direction. In the roughness characterization, the square rod scaffold was the smoothest, while the triangular and circular rod scaffold surfaces were relatively rough, and the circular rod scaffolds were observed to have the highest number of semimolten metal particles. A previous study showed that an implant surface with more semifused particles could increase the probability of bacterial adhesion and colonization, leading to infection, and it also inhibited the osteogenic differentiation of bone marrow mesenchymal stem cells [30].

These results may be related to the SLM processing method. This layer-by-layer powder stacking method has difficulty accurately restoring the model shape of the slope and the continuous surface at the micro-level, and there are tiny sawtooth-like structures between different layers. This local alternating microconcave-convex structure can be sensed by cells through the stretching and relaxation of actin filaments in the cytoskeleton [31]. The influence of curvatures such as these can extend from the cell level to the tissue level and affect physiological activities such as cell proliferation and

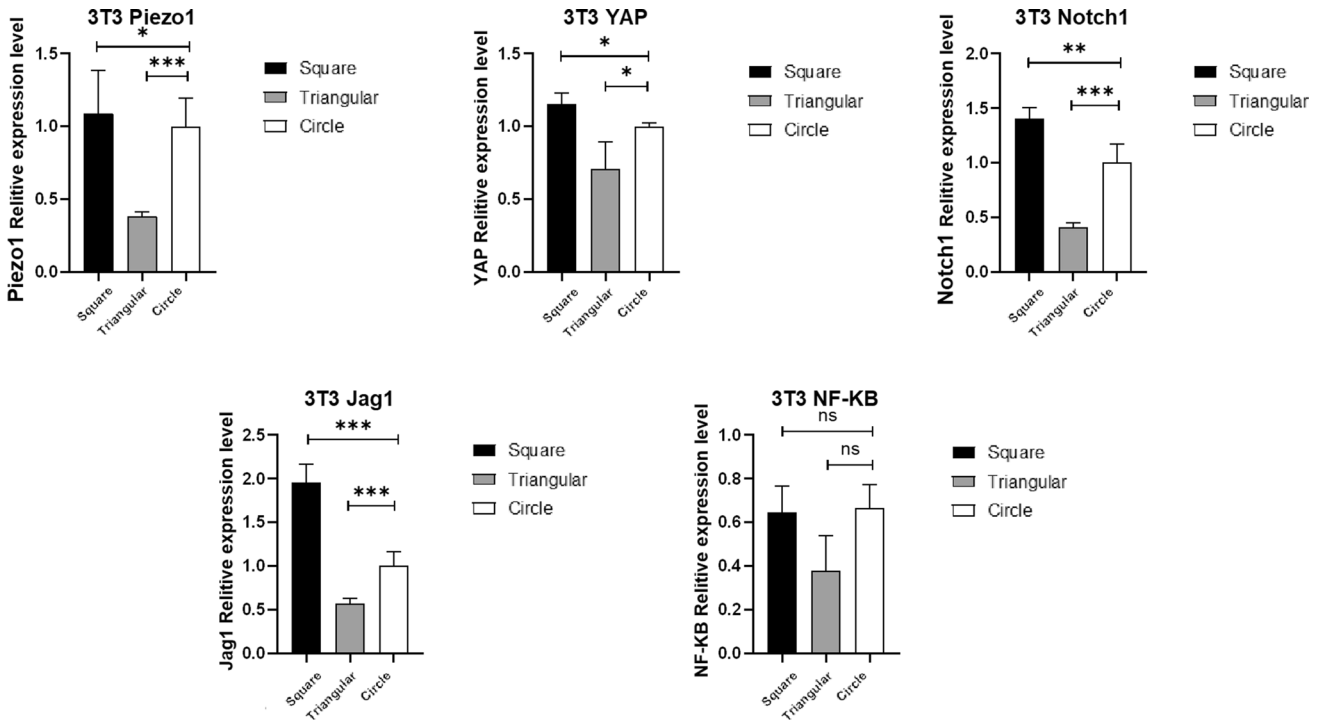

Fig. 9 Relative gene expression levels of MC3T3-E1 cells cultured on scaffolds designed with rods of three different geometric designs after GsMTx4 treated: Relative gene expression levels of Piezo1, YAP, Notch1, Jag1 and NF-KB between three different scaffolds after GsMTx4 treated

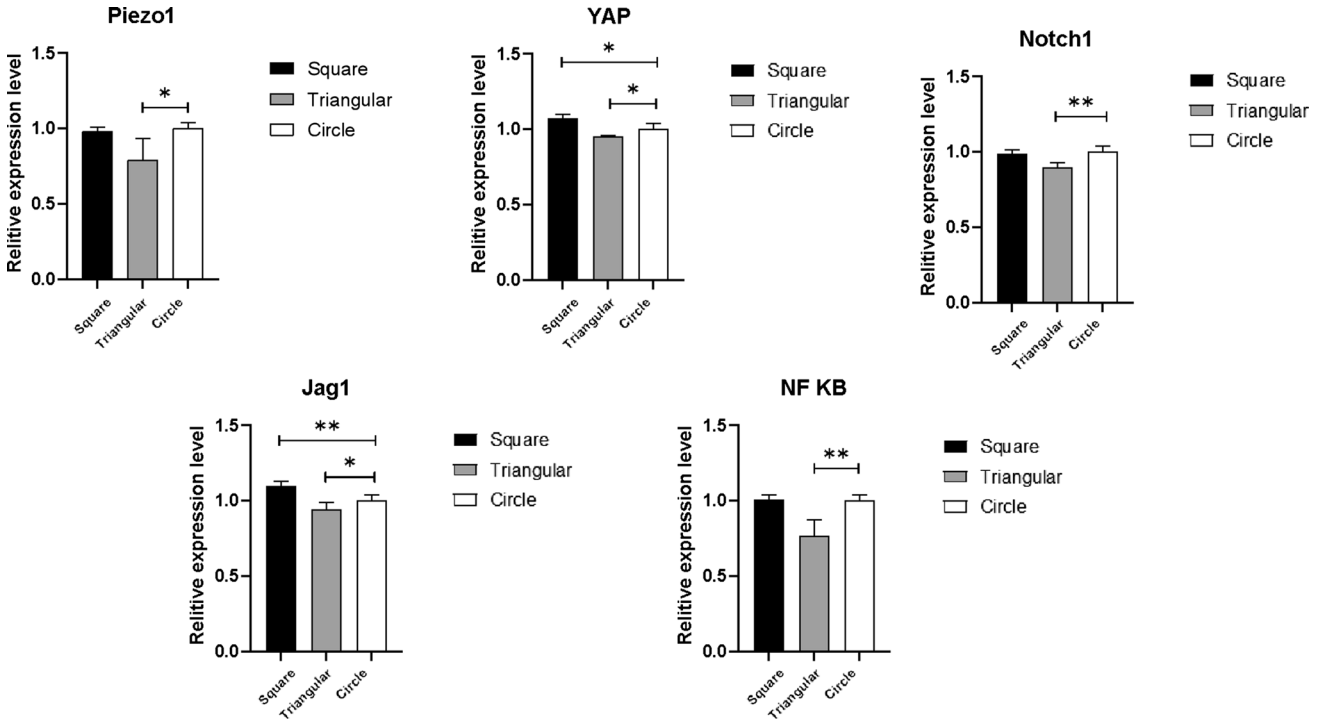

Fig. 10 Relative gene expression levels of MC3T3-E1 cells cultured on scaffolds designed with rods of three different geometric designs after verteporfin treated: Relative gene expression levels of Piezo1, YAP, Notch1, Jag1 and NF-KB between three different scaffolds after verteporfin treated

differentiation [26, 32, 33]. The cell proliferation results in this study may also be related to the effects of these local topographies on the cells.

Three different scaffolds with approximately the same porosity were initially employed in this study, but this situation may lead to the possibility that the three scaffolds may have different pore diameters and different relative surface areas. Therefore, we designed three differently shaped rod scaffolds with approximately the same pore diameter and approximately the same specific surface area and observed similar experimental results. This suggests that the findings are an effect of the scaffold design itself.

Piezo1, an important molecule cells use to sense mechanical signals, is widely expressed in various tissues, such as the nervous, cardiovascular, and musculoskeletal systems [34]. Researchers have found that Piezo1 is involved in the regulation of cell proliferation in a variety of malignancies, including gastric, colon and prostate cancers [35]. Piezo1 is a high-sensitivity channel and can be activated by a variety of mechanical stimuli, such as stretching, shear stress and pulling of the cell membrane and cytoskeleton pulling [36]. Piezo1 has been shown to function in scenarios where cells sense matrix curvature [37].

YAP is another important signalling molecule involved in cell perception of mechanical stimulation. As the core component of the Hippo pathway, YAP/ transcriptional coactivator with PDZ-binding motif (TAZ) plays an important role in cell mechanical signal transduction [38]. Mechanical signals can be used to regulate cell proliferation through this protein, such as cell contact inhibition of proliferation [39]. Swanson et al. found that changes in the scaffold curvature modulate osteogenic differentiation of stem cells via the YAP/TAZ signalling pathway [40]. A previous study also found that the proliferation of MC3T3-E1 cells could be suppressed by Piezo1 activation [41]. The YAP signalling pathway was demonstrated to promote carcinoma cell proliferation via Piezo1 [42].

In recent years, there has been no consensus on the effect of microscopic geometry on YAP signalling, and, thus, on cell proliferation and differentiation. Liu et al. found that the proliferation and differentiation of MC3T3-E1 cells were promoted by a high-curvature triangular pore structure through increasing YAP nuclear translocation [43]. In our study, the square design made each rod has four right angles, resulting in a high curvature topography, and it promoted MC3T3-E1 cell proliferation, which may be caused by a similar mechanism.

Li et al. discovered that the promoting effect of β-catenin on MC3T3-E1 cell proliferation and differentiation was enhanced by a decrease in cytoplasmic YAP levels mediated by autophagy [44]. Therefore, the Piezo1 pathway inhibitor GsMTx4 and the YAP inhibitor verteporfin were selected to treat cells in our study [45–47].

In this study, the trend of cell proliferation after treatment with GsmTx4 or verteporfin was reversed or narrowed compared with that before treatment (Fig. 8). In MC3T3-E1 cells, the square rod scaffolds were observed to have a lower relative Piezo1 gene expression level among the three different design scaffolds (Fig. 7), and it also had the highest cell proliferation velocity, which may be due to lower Piezo1 expression impairing cell contact inhibition. This corresponded to the patterns of cell proliferation seen in the different groups, and after treatment with the inhibitors, the cell proliferation patterns were reversed or narrowed (Figs. 9 and 10).

The activation of Notch1 signalling could negatively regulate the proliferation and differentiation of MC3T3-E1 cells [48], which is consistent with the results of the relatively low expression of Notch1 and higher proliferation levels of cells cocultured with square rod scaffolds. In this study, the differences in Piezo1 and YAP relative gene expression levels are most likely caused by the design of the scaffold rods with different geometric shapes, which show different biological effects on MC3T3-E1 cells.

Therefore, we can conclude that Piezo1 and YAP/TAZ may serve as the key regulatory nodes of this proliferative tendency caused by scaffold geometry changes.

Although our study revealed the proliferation of the MC3T3-E1 cell line on scaffolds with different geometry rod designs, the direct mechanism by which scaffold geometry regulates cell behaviour is not clear. Additional research is necessary to discover which downstream signalling molecules are activated by the Piezo1 and YAP signalling pathways when changes in scaffold geometry are sensed by cells. In the future, we need to carry out an in vivo test to confirm the results we obtained in this study.

5 Conclusion

In our study, three scaffolds with different geometry rod designs were compared after coculture with MC3T3-E1 cells. We found that the MC3T3-E1 cell line had the highest cell proliferation rate on the square rod scaffold, and this finding was valid after controlling for pore size and specific surface area. This could be related to the Piezo1 and YAP/TAZ signalling pathways. At the same porosity, the square rod design has a suitable advantage in compressive strength and elastic modulus over the other rod geometries. Combined with its good biological performance, the square rod scaffold is a promising new design for porous orthopaedic implant medical devices.

Acknowledgements This study was carried out at the 3D Printing Innovation Research Centre of the Ninth People's Hospital Affiliated

to the School of Medicine of Shanghai Jiao Tong University, and the authors thank the founding support from the Shanghai Municipal Key Clinical Specialty–Biomedical Materials (shslczdzk06701), the 3-year Action Plan of Shen kang Development Centre (SHDC2020CR2019B), the Huangpu District Industrial Support Fund (XK2020009), the Shanghai Engineering Research Centre of Innovative Orthopedic Instruments and Personalized Medicine (19DZ2250200) and the Industry Standard Study on 3D Printing Personalized Titanium Alloy Pelvic Reconstruction Prosthesis (21DZ2201500).

Declarations

Conflict of interest The authors state that there are no conflicts of interest to disclose.

References

[1] C. Ma, T. Du, X. Niu, Y. Fan, Bone Res. **10**, 59 (2022)
[2] K. Choi, J.L. Kuhn, M.J. Ciarelli, S.A. Goldstein, J. Biomech. **23**, 1103 (1990)
[3] Y. Heriveaux, S. Le Cann, M. Fraulob, E. Vennat, V.H. Nguyen, G. Haiat, Med. Biol. Eng. Comput. **60**, 3281 (2022)
[4] P. Wang, F.H. Chen, J. Eckert, S. Pilz, K.G. Prashanth, J. Cent, South Univ. **28**, 1068 (2021)
[5] S.J. Yu, P. Wang, H.C. Li, R. Setchi, M.W. Wu, Z.Y. Liu, Z.W. Chen, S. Waqar, L.C. Zhang, Virtual Phys. Prototyp. **18**, e2155197 (2023)
[6] R. Baptista, M. Guedes, J. Mech. Behav. Biomed. Mater. **117**, 104378 (2021)
[7] S. Arabnejad, R. Burnett Johnston, J.A. Pura, B. Singh, M. Tanzer, D. Pasini, Acta Biomater. **30**, 345 (2016)
[8] G. Li, L. Wang, W. Pan, F. Yang, W. Jiang, X. Wu, X. Kong, K. Dai, Y. Hao, Sci. Rep. **6**, 34072 (2016)
[9] C.M. Bidan, K.P. Kommareddy, M. Rumpler, P. Kollmannsberger, P. Fratzl, J.W. Dunlop, Adv. Healthc. Mater. **2**, 186 (2013)
[10] S.J.P. Callens, R.J.C. Uyttendaele, L.E. Fratila-Apachitei, A.A. Zadpoor, Biomaterials **232**, 119739 (2020)
[11] Q. Wang, Y. Huang, Z. Qian, J. Biomed. Nanotechnol. **14**, 628 (2018)
[12] C. Hou, J. An, D. Zhao, X. Ma, W. Zhang, W. Zhao, M. Wu, Z. Zhang, F. Yuan, Front. Bioeng. Biotechnol. **10**, 835008 (2022)
[13] J.O. Abaricia, A.H. Shah, M. Chaubal, K.M. Hotchkiss, R. Olivares-Navarrete, Biomaterials **243**, 119920 (2020)
[14] S. Zhang, Y. Wang, B. Zhou, F. Meng, H. Zhang, S.J. Li, Q.M. Hu, L. Zhou, Acta Metall. Sin. -Engl. Lett. **36**, 35 (2023)
[15] D. Martinez-Marquez, Y. Delmar, S. Sun, R.A. Stewart, Materials (Basel) **13**, 4794 (2020)
[16] M. Alana, A. Lopez-Arancibia, S. Ghouse, N. Rodriguez-Florez, S. Ruiz de Galarreta, Comput. Biol. Med. **150**, 105761 (2022)
[17] J. Parthasarathy, B. Starly, S. Raman, A. Christensen, J. Mech. Behav. Biomed. Mater. **3**, 249 (2010)
[18] W.M. Peng, Y.F. Liu, X.F. Jiang, X.T. Dong, J. Jun, D.A. Baur, J.J. Xu, H. Pan, X. Xu, J. Zhejiang Univ. Sci. B **20**, 647 (2019)
[19] R. Thibeaux, H. Duval, B. Smaniotto, E. Vennat, D. Neron, B. David, Biotechnol. Prog. **35**, 2880 (2019)
[20] C.H. Seo, K. Furukawa, Y. Suzuki, N. Kasagi, T. Ichiki, T. Ushida, Macromol. Biosci. **11**, 938 (2011)
[21] Y. Sun, B. Wan, R. Wang, B. Zhang, P. Luo, D. Wang, J.J. Nie, D. Chen, X. Wu, Front. Cell Dev. Biol. **10**, 808303 (2022)
[22] W. Li, F. Dai, S. Zhang, F. Xu, Z. Xu, S. Liao, L. Zeng, L. Song, F. Ai, ACS Appl. Mater. Interfaces **14**, 20693 (2022)
[23] V. Karageorgiou, D. Kaplan, Biomaterials **26**, 5474 (2005)
[24] D.J. Lee, J. Kwon, Y.I. Kim, X. Wang, T.J. Wu, Y.T. Lee, S. Kim, P. Miguez, C.C. Ko, Orthod. Craniofac. Res. **22**(Suppl 1), 127 (2019)
[25] S. Ehrig, B. Schamberger, C.M. Bidan, A. West, C. Jacobi, K. Lam, P. Kollmannsberger, A. Petersen, P. Tomancak, K. Kommareddy, F.D. Fischer, P. Fratzl, J.W.C. Dunlop, Sci. Adv. **5**, 1 (2019). https://doi.org/10.1126/sciadv.aav9394
[26] M. Werner, N.A. Kurniawan, C.V.C. Bouten, Materials (Basel) **13**, 963 (2020)
[27] D. Martinez-Moreno, G. Jimenez, C. Chocarro-Wrona, E. Carrillo, E. Montanez, C. Galocha-Leon, B. Clares-Naveros, P. Galvez-Martin, G. Rus, J. de Vicente, J.A. Marchal, Mater. Sci. Eng. C Mater. Biol. Appl. **122**, 111933 (2021)
[28] J. Hu, S. Wang, B. Li, F. Li, Z. Luo, L. Liu, IEEE. Trans. Vis Comput. Graph. **28**, 2615 (2022)
[29] D.A. Muller, U. Silvan, Int. J. Dev. Biol. **63**, 1 (2019)
[30] K. Xie, Y. Guo, S. Zhao, L. Wang, J. Wu, J. Tan, Y. Yang, W. Wu, W. Jiang, Y. Hao, Clin. Orthop. Relat. Res. **477**, 2772 (2019)
[31] K.A. DeMali, X. Sun, G.A. Bui, Biochemistry **53**, 7706 (2014)
[32] M. Paris, A. Gotz, I. Hettrich, C.M. Bidan, J.W.C. Dunlop, H. Razi, I. Zizak, D.W. Hutmacher, P. Fratzl, G.N. Duda, W. Wagermaier, A. Cipitria, Acta Biomater. **60**, 64 (2017)
[33] S.M. Yu, J.M. Oh, J. Lee, W. Lee-Kwon, W. Jung, F. Amblard, S. Granick, Y.K. Cho, Acta Biomater. **77**, 311 (2018)
[34] X.Z. Fang, T. Zhou, J.Q. Xu, Y.X. Wang, M.M. Sun, Y.J. He, S.W. Pan, W. Xiong, Z.K. Peng, X.H. Gao, Y. Shang, Cell Biosci. **11**, 13 (2021)
[35] J.L. Yu, H.Y. Liao, Biomed. Pharmacother. **140**, 111692 (2021)
[36] Y. Jiang, X. Yang, J. Jiang, B. Xiao, Trends Biochem. Sci. **46**, 472 (2021)
[37] A.H. Lewis, J. Grandl, Elife **4**, 12088 (2015)
[38] M. Fu, Y. Hu, T. Lan, K.L. Guan, T. Luo, M. Luo, Signal Transduct. Target. Ther. **7**, 376 (2022)
[39] M. Aragona, T. Panciera, A. Manfrin, S. Giulitti, F. Michielin, N. Elvassore, S. Dupont, S. Piccolo, Cell **154**, 1047 (2013)
[40] W.B. Swanson, M. Omi, S.M. Woodbury, L.M. Douglas, M. Eberle, P.X. Ma, N.E. Hatch, Y. Mishina, Int. J. Mol. Sci. **23**, 4499 (2022)
[41] M. Yoneda, H. Suzuki, N. Hatano, S. Nakano, Y. Muraki, K. Miyazawa, S. Goto, K. Muraki, Int. J. Mol. Sci. **20**, 4960 (2019)
[42] K. Hasegawa, S. Fujii, S. Matsumoto, Y. Tajiri, A. Kikuchi, T. Kiyoshima, J. Pathol. **253**, 80 (2021)
[43] Y. Liu, Q. Yang, Y. Wang, M. Lin, Y. Tong, H. Huang, C. Yang, J. Wu, B. Tang, J. Bai, C. Liu, A.C.S. Biomater, Sci. Eng. **8**, 3498 (2022)
[44] L. Li, S. Yang, L. Xu, Y. Li, Y. Fu, H. Zhang, J. Song, Acta Biomater. **96**, 674 (2019)
[45] C. Bae, F. Sachs, P.A. Gottlieb, Biochemistry **50**, 6295 (2011)
[46] K. Vigneswaran, N.H. Boyd, S.Y. Oh, S. Lallani, A. Boucher, S.G. Neill, J.J. Olson, R.D. Read, Clin. Cancer Res. **27**, 1553 (2021)
[47] H. Wei, F. Wang, Y. Wang, T. Li, P. Xiu, J. Zhong, X. Sun, J. Li, Cancer Sci. **108**, 478 (2017)
[48] Y. Xu, L. Li, Y. Tang, J. Yang, Y. Jin, C. Ma, Eur. J. Pharmacol. **865**, 172794 (2019)